Chemical Science

ROYAL SOCIETY OF CHEMISTRY

EDGE ARTICLE

View Article Online
View Journal | View Issue

Cite this: *Chem. Sci.*, 2022, **13**, 5171

All publication charges for this article have been paid for by the Royal Society of Chemistry

Received 14th February 2022
Accepted 8th April 2022

DOI: 10.1039/d2sc00960a

rsc.li/chemical-science

$[Ni_{30}S_{16}(PEt_3)_{11}]$: an open-shell nickel sulfide nanocluster with a "metal-like" core†

Alexander J. Touchton, Guang Wu and Trevor W. Hayton *

Reaction of $[Ni(1,5\text{-cod})_2]$ (30 equiv.) with PEt_3 (46 equiv.) and S_8 (1.9 equiv.) in toluene, followed by heating at 115 °C for 16 h, results in the formation of the atomically precise nanocluster (APNC), $[Ni_{30}S_{16}(PEt_3)_{11}]$ (**1**), in 14% isolated yield. Complex **1** represents the largest open-shell Ni APNC yet isolated. In the solid state, **1** features a compact "metal-like" core indicative of a high degree of Ni–Ni bonding. Additionally, SQUID magnetometry suggests that **1** possesses a manifold of closely-spaced electronic states near the HOMO–LUMO gap. *In situ* monitoring by ESI-MS and $^{31}P\{^1H\}$ NMR spectroscopy reveal that **1** forms *via* the intermediacy of smaller APNCs, including $[Ni_8S_5(PEt_3)_7]$ and $[Ni_{26}S_{14}(PEt_3)_{10}]$ (**2**). The latter APNC was also characterized by X-ray crystallography and features a nearly identical core structure to that found in **1**. This work demonstrates that large APNCs with a high degree of metal–metal bonding are isolable for nickel, and not just the noble metals.

Introduction

Atomically-precise nanoclusters (APNCs) are an emerging class of materials that feature properties found in both metal complexes and bulk metal.[1] Unlike traditional nanoparticles, APNCs are perfectly monodisperse and feature a well-defined arrangement of their capping ligands.[2,3] This high level of chemical precision makes them attractive for a variety of applications,[4] including catalysis,[5–7] sensing,[8] and imaging.[8,9] Magnetic APNCs, in particular, have been touted as alternatives to larger ferromagnetic nanoparticles for use in existing technologies, like magnetic data storage,[10] and frontier technologies, like quantum computing.[11,12] However, very little APNC research has focused on ferromagnetic metals, such as Fe, Co, and Ni, and so these applications have yet to be realized. Indeed, the vast majority of APNC work has focused on the group 11 metals, which tend to generate diamagnetic APNCs.[5,13]

Nonetheless, some past work has shown that open-shell APNCs of Ni are isolable.[14] For example, $[Ni_9Te_6(PEt_3)_8]$, first reported in 1989,[15] features an $S = 2$ ground state.[16–18] Similarly, the mixed-metal cluster $[NBu_4]_4[Ni_{16}Pd_{16}(CO)_{40}]$, features a $J = 2$ ground state.[19] In addition, we recently reported the isolation of $[Ni_{23}Se_{12}Cl_3(PEt_3)_{10}]$,[20–22] which features an $S = 3/2$ ground state according to an Evans' method determination. Also notable are calculations of $[Ni_{44}(CO)_{48}]^{6-}$,[23–25] which predict an open shell ground state. Notably, the unpaired electron density in $[Ni_{44}(CO)_{48}]^{6-}$ was calculated to reside exclusively on the six core Ni atoms, which exhibit fcc-type packing. Intriguingly, $[Ni_{23}Se_{12}Cl_3(PEt_3)_{10}]$ also features fcc packing of its central Ni_{13} core.[20,21] While its electronic structure is not entirely understood, we propose that its paramagnetism is related to this metal-like core structure. Moreover, we hypothesize that larger nickel chalcogenide APNCs will feature greater structural similarity to bulk Ni, potentially resulting in the emergence of superparamagnetic or ferromagnetic behaviour. The resulting APNCs would be potentially useful in a number of magnetic applications.[12,26]

In an effort to test this hypothesis, we endeavoured to synthesize and characterize even larger open-shell Ni APNCs. Herein, we report the largest open-shell Ni APNC yet known, namely, $[Ni_{30}S_{16}(PEt_3)_{11}]$ (**1**). X-ray crystallography reveals a compact "metal-like" core indicating a high degree of Ni–Ni bonding. Additionally, SQUID magnetometry shows that **1** possesses an open shell ground state.

Results and discussion

Previous attempts by our research group to form large Ni APNCs demonstrated that low-valent Ni nanoclusters are incompatible with Ph_3P, which is too easily reduced.[27] Additionally, past work by Jin and co-workers has shown that $NaBH_4$ cannot reduced Ni^{2+} salts to Ni(0).[28–30] Given these considerations, we chose PEt_3 as our supporting ligand and $[Ni(1,5\text{-cod})_2]$ as our Ni source. Thus, heating a mixture of $[Ni(1,5\text{-cod})_2]$ (30 equiv.), PEt_3 (46 equiv.), and S_8 (1.9 equiv.) in toluene at 115 °C for 16 h generated a deep brown solution. Work-up of the reaction mixture afforded $[Ni_{30}S_{16}(PEt_3)_{11}]$ (**1**) as a black crystalline solid in 14%

Department of Chemistry and Biochemistry, University of California, Santa Barbara, California 93106, USA. E-mail: hayton@chem.ucsb.edu

† Electronic supplementary information (ESI) available: Experimental procedures, crystallographic details (as CIF files), computational results, and spectral data for complexes **1**·Et_2O and **2**·C_5H_{12}. CCDC 2150613 and 2150614. For ESI and crystallographic data in CIF or other electronic format see https://doi.org/10.1039/d2sc00960a

yield. Air-sensitive **1** is soluble in toluene, benzene, and THF, very sparingly soluble in hexanes, pentane, methylene chloride, diethyl ether, and 1,2-dimethoxyethane, and insoluble in acetonitrile. C_6D_6 solutions of **1** exhibit complete decomposition upon exposure to air and water after 18 h (Fig. S44 and S45†).

Curiously, the highest yields of **1** were achieved with an Ni : PEt_3 ratio of *ca.* 1 : 1.5. When the Ni : PEt_3 ratio was decreased to 3 : 1 (the rational stoichiometry, given the formula of **1**) the isolated yields were reduced substantially. Previous work by our group suggests that the first step in APNC formation involves formation of $[Ni(1,5\text{-cod})(PEt_3)_2]$ by ligand substitution.[30] Thus, we surmise that a large excess of PEt_3 is required to completely form $[Ni(1,5\text{-cod})(PEt_3)_2]$, which is much more thermally stable than $[Ni(1,5\text{-cod})_2]$, and subsequently functions as a better Ni(0) source at these elevated temperatures. However, the excess PEt_3 unavoidably sequesters some of the S_8 (see below), which likely contributes to the low isolated yield.

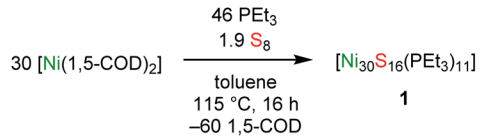

Single crystals of **1** were grown by slow evaporation of a cold (−25 °C) toluene/Et_2O solution over the course of three weeks. Complex **1** crystallizes in monoclinic space group $P2_1/n$, as the diethyl ether solvate, **1**·Et_2O (Fig. 1). The solid-state structure of **1** consists of a densely packed core with extensive Ni–Ni bonding. The core is anchored by two interpenetrating Ni_{13} "kernels" (Fig. 1A and B). Curiously, neither kernel adopts the archetypal cuboctahedral (fcc) or anti-cuboctahedral (hcp) geometries observed for many Au APNCs.[13] Instead, they adopt an irregular arrangement of their Ni atoms. The resulting Ni_{21} polyhedron is capped by three "[*cyclo*-{Ni(μ-S)(PEt_3)}$_3$]" units (Fig. 1C and D). Two of these units are equivalent by symmetry. Similar "[*cyclo*-{Ni(μ-E)(PEt_3)}$_3$]" units are found in $[Ni_{23}Se_{12}Cl_3(PEt_3)_{10}]$.[20] The addition of these three capping units brings the total metal nuclearity to 30 (Fig. 1E and F). Also appended to the Ni_{21} polyhedron are two PEt_3 ligands (at Ni28 and Ni15), five μ_4-S^{2-} ligands, and two μ_5-S^{2-} ligands, giving this Ni_{30} cluster an overall C_s symmetric structure (Fig. 1G, H and S46†).

As a result of this arrangement, five Ni atoms (Ni1, Ni2, Ni3, Ni4, Ni5) feature coordination numbers of 11 or greater, and two Ni atoms are solely bonded to other Ni atoms (Ni1 and Ni3) (Fig. S46†). The high coordination numbers exhibited by these atoms is reminiscent of bulk Ni, which features coordination number of 12.[31,32] No other Ni APNC features comparable amounts of "metal-like" character. For comparison, only two other reported Ni nanoclusters feature compact "metal-like" cores, namely, $[Ni_{21}Se_{14}(PEt_2Ph)_{12}]$ and $[Ni_{23}Se_{12}Cl_3(PEt_3)_{10}]$, which each have just one fcc and hcp Ni_{13} "kernel", respectively.[20,33] This paucity of examples lies in stark contrast to the broad landscape of "metal-like" structures observed for Ag and Au. Indeed, over 250+ high-nuclearity, low-valent group 11 APNCs have been structurally characterized over the last 10 years.[34]

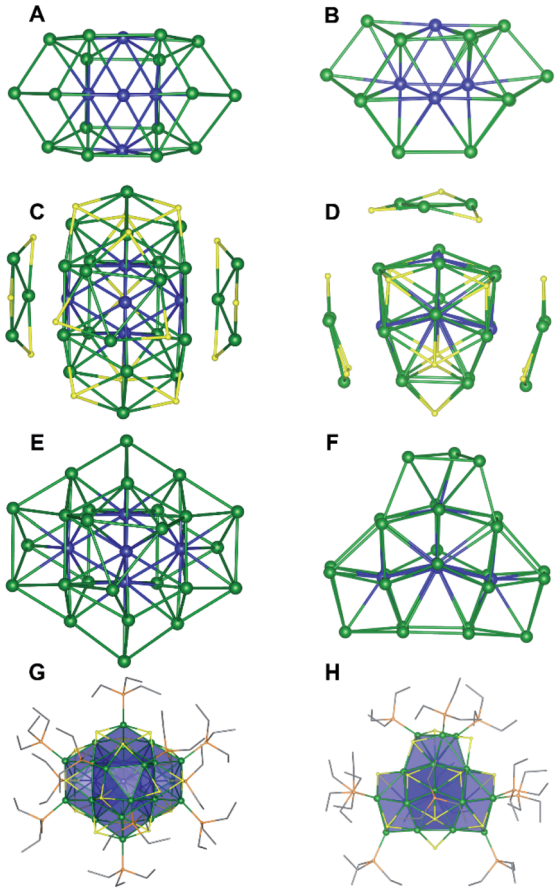

Fig. 1 Solid-state structure of $[Ni_{30}S_{16}(PEt_3)_{11}]\cdot Et_2O$ (**1**·Et_2O) from two different orientations. (A and B) Ni_{21} core. (C and D) The three [*cyclo*-{Ni(μ-S)}$_3$] units attached to the $Ni_{21}S_7$ core. (E and F) Ni-only structure of **1**. (G and H) Full molecular structure. Color scheme: Ni_{shell}, green; Ni_{core}, blue; S, yellow; P, orange; C, grey. Carbon atoms are shown in wireframe. Diethyl ether solvate molecule and hydrogen atoms were omitted for clarity.

The 99 Ni–Ni distances in **1** span a large range (2.401(3)–2.911(3) Å), which is typical of APNCs,[7,35] and the average Ni–Ni distance is 2.58 Å. A histogram of these distances (Fig. S1†) shows the highest frequency from 2.40 and 2.55 Å, which compares well to the Ni–Ni distance in bulk Ni metal (2.49 Å).[31,32] The 68 Ni–S distances in **1** also span a large range (2.104(5)–2.759(4) Å) with an average of 2.24 Å. A histogram of these distances (Fig. S2†) shows the highest frequency between 2.20 Å and 2.25 Å. For comparison, the average Ni–S distances observed in $[Ni_5S_2(SPh)_2(PEt_3)_5]$ and $[Ni_8S_5(PEt_3)_7]$ are shorter (2.04 and 2.19 Å, respectively), perhaps reflecting the lower average coordination number of their S^{2-} ligands.[30] For further comparison, the average Ni–S distance in β-NiS is 2.31 Å,[36] whereas the Ni–S distances in Ni_3S_2 are 2.2914(5) and 2.2534(5) Å.[37] Finally, the average Ni–P distance in **1** is 2.18 Å, which is similar to Ni–P distances in $[Ni_8S_5(PEt_3)_7]$, $[Ni_{21}Se_{14}(PEt_2Ph)_{12}]$, and $[Ni_{23}Se_{12}Cl_3(PEt_3)_{10}]$.[20,30,33]

The average Ni oxidation state in **1** is 1.067, making it among the most reduced Ni chalcogenide clusters yet isolated, and highlighting its high "metal-like" character. For comparison,

$[Ni_{32}S_{24}(PPh_3)_{10}]$, $[Ni_8S_5(PEt_3)_7]$, $[Ni_{21}Se_{14}(PEt_2Ph)_{12}]$, and $[Ni_{23}Se_{12}Cl_3(PEt_3)_{10}]$ have average oxidation states of 1.5, 1.25, 1.33, and 1.17, respectively.[20,30,33,38] Despite its low average oxidation state, the disparate coordination geometries of the interior Ni atoms *vs.* the surface Ni atoms in **1** suggest that the oxidation load is not distributed evenly over all 30 Ni atoms. In this regard, we hypothesize that the oxidation states of five interior Ni atoms approach 0, whereas the oxidation states of surface Ni atoms are closer to 2+.

The $^{31}P\{^1H\}$ NMR spectrum of **1** in toluene-d_8 displays resonances at 30, 246, 842, and 2054 ppm, in a 4 : 2 : 3 : 2 ratio, respectively (Fig. 2A and S18–S20†).[39] While these results confirm the presence of 11 PEt_3 ligands, they contrast with the pattern expected for a complex with C_s symmetry, which should feature seven peaks in a 1 : 1 : 1 : 2 : 2 : 2 : 2 ratio. To explain this discrepancy, we propose that the unique "[*cyclo*-{Ni(μ-S)$(PEt_3)\}_3$]" unit (comprised of Ni26, Ni29, and Ni30), can rotate with respect to the Ni_{21} polyhedron, giving **1** an effective symmetry of C_{2v}. Cooling a sample of **1** in toluene-d_8 to −25 °C results in shifting of four PEt_3 resonances (Fig. S21–S23†), but no decoalescence of these peaks was observed. However, plots of these shifts *vs.* T^{-1} are linear, demonstrating the Curie–Weiss behavior expected for a paramagnet (Fig. 2B and S24†).[40] The electrospray ionization mass spectrum (ESI-MS) of **1**, recorded in THF in positive ion mode, features two major peaks at 3572.43 *m*/*z* and 1786.20 *m*/*z* (Fig. 2D and S26–S28†), which correspond to $[Ni_{30}S_{16}(PEt_3)_{11}]^+$ (calcd 3572.57 *m*/*z*) and $[Ni_{30}S_{16}(PEt_3)_{11}]^{2+}$ (calcd 1787.30 *m*/*z*), respectively. Overall, these results further confirm our proposed formulation.

To further probe its magnetic properties, we measured the moment of **1** in solution *via* Evans' method and in the solid state *via* variable-temperature SQUID magnetometry. Complex **1** exhibits a magnetic moment of 2.70 cm^3 K mol^{-1} at 298 K in C_6D_6.[41,42] In the solid state, its magnetic moment is 2.53 cm^3 K mol^{-1} at 300 K (Fig. 2C and S43†). This value drops to 1.38 cm^3 K mol^{-1} on cooling to 100 K, briefly plateaus, then drops to 0.33 cm^3 K mol^{-1} at 2 K. These data are consistent with the field-induced mixing of a triplet ground state with a low-lying quintet excited state and can be rationalized by a manifold of closely-spaced electronic states near the HOMO–LUMO gap, as expected for an APNC with a high degree of metal–metal bonding. Additionally, zero-field-cooled (ZFC) and field-cooled (FC) magnetization *vs.* temperature curves indicate no magnetic blocking down to 1.8 K, while no hysteresis is seen when cycling magnetization *vs.* applied field (Fig. S39 and S42†).

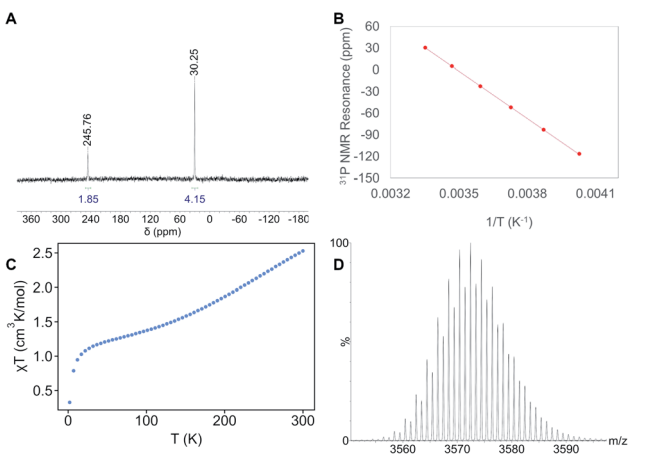

Fig. 2 Characterization data for **1**. (A) Partial $^{31}P\{^1H\}$ NMR spectrum of **1** in toluene-d_8. (B) A plot of $^{31}P\{^1H\}$ NMR chemical shift *versus* T^{-1} for the 30 ppm (25 °C) resonance. (C) Variable temperature magnetic susceptibility (χT) for **1** collected at 10 000 Oe. (D) Partial ESI-MS mass spectrum of **1** in THF (capillary voltage of 2.50 kV, positive ion mode) showing a peak at 3572.43 *m*/*z* assignable to $[Ni_{30}S_{16}(PEt_3)_{11}]^+$ (calcd 3572.57 *m*/*z*).

To better understand its synthesis, we monitored the *in situ* formation of **1** by ESI-MS, as well as by $^{31}P\{^1H\}$ and ^1H NMR spectroscopies (Fig. S5–S15†). A mass spectrum of a reaction aliquot, collected immediately after mixing the reagents, features a major peak at 1456.0 *m*/*z* that is assignable to $[Ni_8S_5(PEt_3)_7]^+$ (calcd 1455.97 *m*/*z*).[30] A mass spectrum recorded after heating the reaction mixture to 115 °C for 105 min also features the peak assignable to $[Ni_8S_5(PEt_3)_7]^+$. However, this spectrum features several additional peaks, which are assignable to $[Ni_{20}S_{12}(PEt_3)_7]^+$, $[Ni_{21}S_{14}(PEt_3)_7]^+$, $[Ni_{21}S_{14}(PEt_3)_8]^+$, $[Ni_{23}S_{14}(PEt_3)_9]^+$, $[Ni_{26}S_{14}(PEt_3)_{10}]^+$ ($[\mathbf{2}]^+$), and $[Ni_{30}S_{16}(PEt_3)_{11}]^+$ ($[\mathbf{1}]^+$). Heating of the reaction mixture for 17 h results in a sharp decrease of the peaks assignable to the Ni_8–Ni_{26} clusters in the ESI-MS, leaving **1** as the major remaining high molecular weight material.[43] The *in situ* $^{31}P\{^1H\}$ and ^1H NMR spectra corroborate the reaction trajectory suggested by the ESI-MS data (Fig. S10–S15†). The NMR spectra reveal that Et_3PS is also formed in the reaction. Overall, these data suggest that $[Ni_8S_5(PEt_3)_7]^+$, $[Ni_{20}S_{12}(PEt_3)_7]^+$, $[Ni_{21}S_{14}(PEt_3)_7]^+$, $[Ni_{21}S_{14}(PEt_3)_8]^+$, $[Ni_{23}S_{14}(PEt_3)_9]^+$, and $[Ni_{26}S_{14}(PEt_3)_{10}]^+$ are likely intermediates in the formation of **1**, and that cluster growth is promoted by longer reaction times and high temperatures.

We next sought to isolate one of the intermediately-sized Ni nanoclusters that we observed in the *in situ* ESI mass spectra. To target these intermediates, we decreased the reaction temperature and shortened the reaction time. Thus, thermolysis of a mixture of $[Ni(1,5\text{-cod})_2]$ (30 equiv.), PEt_3 (31 equiv.), and S_8 (1.9 equiv.) in toluene at 95 °C for 5 h provided a complex mixture containing **1**, **2**, $[Ni_8S_5(PEt_3)_7]$, and Et_3PS, as assayed by $^{31}P\{^1H\}$ NMR spectroscopy (Fig. S37†). Work-up of this mixture afforded relatively pure $[Ni_{26}S_{14}(PEt_3)_{10}]$ (**2**) in 5% yield *via* selective crystallization. However, the isolated material also contained a small amount of complex **1**, which precluded its complete characterization. Complex **2** is very soluble in tetrahydrofuran, toluene, and benzene, but is sparingly soluble in pentane, hexanes, and diethyl ether.

Single crystals of **2** were grown by slow evaporation of a cold (−25 °C) toluene/pentane solution over the course of one week. They crystallize in the monoclinic space group $P2_1/n$ as the pentane solvate, $\mathbf{2}\cdot C_5H_{12}$ (Fig. 3 and S47†). The solid-state structure of **2** is remarkably similar to that of complex **1** and can be derived from that of **1** by removal of one "[*cyclo*-{Ni(μ-S)$(PEt_3)\}_3$]" unit and substitution of Ni5 with a μ_6-S^{2-} ligand. The positions of the remaining Ni atoms are unchanged. Not surprisingly, then, the metrical parameters of **2** are similar to those of **1**. For example, the average Ni–Ni distance in **2** (2.56 Å)

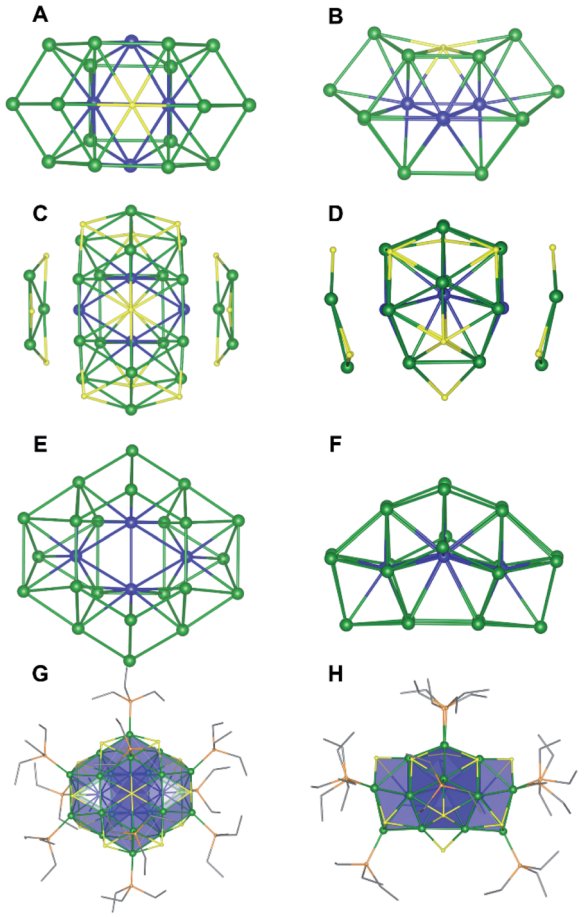

Fig. 3 Solid-state structure of $[Ni_{26}S_{14}(PEt_3)_{10}]\cdot C_5H_{12}$ ($\mathbf{2}\cdot C_5H_{12}$) from two different orientations. (A and B) $Ni_{20}S$ core. (C and D) The two [*cyclo*-{Ni(μ-S)}$_3$] units attached to the $Ni_{20}S_8$ core. (E and F) Ni-only structure of **2**. (G and H) Full molecular structure. Color scheme: Ni_{shell}, green; Ni_{core}, blue; S, yellow; P, orange; C, grey. Carbon atoms are shown in wireframe. Pentane solvate molecule and hydrogen atoms were omitted for clarity.

is similar to that of **1**, and the values span a similar range (2.399(6)–2.889(7) Å).

The $^{31}P\{^1H\}$ NMR spectrum of **2** in C_6D_6 features resonances at 5730, 912, 606, and 179 ppm (Fig. S31 and S32†). The latter three resonances are present in a 2 : 2 : 4 ratio. The number and intensities of the resonances are consistent with the C_{2v} symmetry observed in the solid state, while the large downfield chemical shifts are suggestive of a paramagnetic ground state. The ^1H NMR spectrum of **2** in C_6D_6 is also indicative of a paramagnetic cluster, as revealed by a resonance at 21.38 ppm that is assignable to a PEt_3 methylene environment (Fig. S30†). Finally, the ESI-MS of **2** in THF (positive ion mode) features a major peak at 3155.05 *m*/*z* (Fig. S34†), which corresponds to $[Ni_{26}S_{14}(PEt_3)_{10}]^+$ (calcd 3154.80 *m*/*z*), further confirming our formulation.

Formally, conversion of **2** into **1** requires addition of 4 equiv. of "Ni(0)", 2 equiv. of "S", and 1 equiv. of PEt_3. Surprisingly, however, this change results in minimal rearrangement of the Ni_{26} core. The similarity of their structures supports our contention that **2** is an intermediate in the formation of **1**. Additionally, the similar core structures in **1** and **2** suggests that it is an especially stable fragment and may form a good "seed" for further cluster growth.

Conclusions

In summary, we have isolated the largest open-shell Ni chalcogenide APNC reported to date. X-ray crystallography reveals that this nanocluster contains a compact "metal-like" core that is unprecedented for the group 10 elements. Additionally, SQUID magnetometry measurements suggest a manifold of closely-spaced electronic states near the HOMO–LUMO gap, further corroborating the nanocluster's "metal-like" nature. Importantly, this work shows that large APNCs with a high degree of metal–metal bonding are possible for nickel, and not just the noble metals, opening the door to the synthesis of a much more chemically diverse array of APNCs. These new group 10 APNCs offer promise for their unique, and potentially useful, magnetic properties.

Author contributions

A. J. T. performed the synthesis and characterization. G. W. assisted with the crystallography. A. J. T. and T. W. H. jointly wrote the manuscript. T. W. H. secured funding for the research.

Data availability

All of the experimental data have been included in the ESI. Crystallographic data can be obtained from the CCDC (2150613 and 2150614).†

Conflicts of interest

There are no conflicts to declare.

Acknowledgements

We thank the National Science Foundation (CHE 1764345) for financial support of this work. This research made use of a 500 MHz NMR Spectrometer supported by an NSF Major Research Instrumentation (MRI) Award 1920299. The MRL Shared Experimental Facilities are supported by the MRSEC Program of the National Science Foundation under award NSF DMR 1720256; a member of the NSF-funded Materials Research Facilities Network. A. J. T. thanks the UCSB Eddleman Center for Quantum Innovation for a Graduate Student Support Grant.

Notes and references

1 M. Walter, J. Akola, O. Lopez-Acevedo, P. D. Jadzinsky, G. Calero, C. J. Ackerson, R. L. Whetten, H. Grönbeck and H. Häkkinen, *Proc. Natl. Acad. Sci. U. S. A.*, 2008, **105**, 9157–9162.
2 R. Jin, *Nanoscale*, 2010, **2**, 343–362.

3 X. Kang, H. Chong and M. Zhu, *Nanoscale*, 2018, **10**, 10758–10834.
4 I. Chakraborty and T. Pradeep, *Chem. Rev.*, 2017, **117**, 8208–8271.
5 G. Li and R. Jin, *Acc. Chem. Res.*, 2013, **46**, 1749–1758.
6 L. Liu and A. Corma, *Chem. Rev.*, 2018, **118**, 4981–5079.
7 A. W. Cook, Z. R. Jones, G. Wu, S. L. Scott and T. W. Hayton, *J. Am. Chem. Soc.*, 2018, **140**, 394–400.
8 L.-Y. Chen, C.-W. Wang, Z. Yuan and H.-T. Chang, *Anal. Chem.*, 2015, **87**, 216–229.
9 M. Colombo, S. Carregal-Romero, M. F. Casula, L. Gutierrez, M. P. Morales, I. B. Bohm, J. T. Heverhagen, D. Prosperi and W. J. Parak, *Chem. Soc. Rev.*, 2012, **41**, 4306–4334.
10 C. Busche, L. Vilà-Nadal, J. Yan, H. N. Miras, D.-L. Long, V. P. Georgiev, A. Asenov, R. H. Pedersen, N. Gadegaard, M. M. Mirza, D. J. Paul, J. M. Poblet and L. Cronin, *Nature*, 2014, **515**, 545.
11 N. A. Frey and S. Sun, in *Inorganic Nanoparticles: Synthesis, Application, and Perspective*, CRC Press, Boca Raton, 1st edn, 2010, ch. 3, pp. 33–68, DOI: **10.1201/b10333-3**.
12 A. Gaita-Arino, F. Luis, S. Hill and E. Coronado, *Nat. Chem.*, 2019, **11**, 301–309.
13 R. C. Jin, C. J. Zeng, M. Zhou and Y. X. Chen, *Chem. Rev.*, 2016, **116**, 10346–10413.
14 A. J. Touchton, G. Wu and T. W. Hayton, *J. Chem. Phys.*, 2021, **154**, 211102.
15 J. G. Brennan, T. Siegrist, S. M. Stuczynski and M. L. Steigerwald, *J. Am. Chem. Soc.*, 1989, **111**, 9240–9241.
16 T. T. M. Palstra, M. L. Steigerwald, A. P. Ramirez and J. Zaanen, *Phys. B*, 1994, **199**, 619–621.
17 T. T. M. Palstra, M. L. Steigerwald, A. P. Ramirez, Y. U. Kwon, S. M. Stuczynski, L. F. Schneemeyer, J. V. Waszczak and J. Zaanen, *Phys. Rev. Lett.*, 1993, **71**, 1768–1771.
18 A. C. Reber, V. Chauhan and S. N. Khanna, *J. Chem. Phys.*, 2017, **146**, 024302.
19 M. Riccò, T. Shiroka, S. Carretta, F. Bolzoni, C. Femoni, M. C. Iapalucci and G. Longoni, *Chem. - Eur J.*, 2005, **11**, 2856–2861.
20 A. J. Touchton, G. Wu and T. W. Hayton, *Inorg. Chem.*, 2021, **60**, 17586–17592.
21 J. G. Brennan, T. Siegrist, Y. U. Kwon, S. M. Stuczynski and M. L. Steigerwald, *J. Am. Chem. Soc.*, 1992, **114**, 10334–10338.
22 P. Wix, G. E. Kostakis, V. A. Blatov, D. M. Proserpio, S. P. Perlepes and A. K. Powell, *Eur. J. Inorg. Chem.*, 2013, **2013**, 520–526.
23 N. Rösch, L. Ackermann and G. Pacchioni, *J. Am. Chem. Soc.*, 1992, **114**, 3549–3555.
24 N. Rösch, L. Ackermann, G. Pacchioni and B. I. Dunlap, *J. Chem. Phys.*, 1991, **95**, 7004–7007.
25 L. Ackermann, N. Rösch, B. I. Dunlap and G. Pacchioni, *Int. J. Quantum Chem.*, 1992, **44**, 605–619.
26 J. Nehrkorn, S. M. Greer, B. J. Malbrecht, K. J. Anderton, A. Aliabadi, J. Krzystek, A. Schnegg, K. Holldack, C. Herrmann, T. A. Betley, S. Stoll and S. Hill, *Inorg. Chem.*, 2021, **60**, 4610–4622.
27 A. J. Touchton, G. Wu and T. W. Hayton, *Organometallics*, 2020, **39**, 1360–1365.
28 H. N. Kagalwala, E. Gottlieb, G. Li, T. Li, R. Jin and S. Bernhard, *Inorg. Chem.*, 2013, **52**, 9094–9101.
29 A. W. Cook and T. W. Hayton, *Acc. Chem. Res.*, 2018, **51**, 2456–2464.
30 A. J. Touchton, G. Wu and T. W. Hayton, *Small*, 2021, **17**, 2003133.
31 L. Mazza and A. G. Nasini, *London Edinburgh Philos. Mag. J. Sci.*, 1929, **7**, 301–311.
32 J. Bandyopadhyay and K. P. Gupta, *Cryogenics*, 1977, **17**, 345–347.
33 D. Fenske, H. Krautscheid and M. Müller, *Angew. Chem., Int. Ed. Engl.*, 1992, **31**, 321–323.
34 Data taken from a search of the Cambridge Structural Database (CSD), Version 5.42 (September 2021 update). Defined here as a cluster that contains at least one group 11 atom coordinated to at least eight other group 11 atoms and no non-metal atoms. The search was restricted to homometallic APNCs.
35 T. A. Nguyen, Z. R. Jones, B. R. Goldsmith, W. R. Buratto, G. Wu, S. L. Scott and T. W. Hayton, *J. Am. Chem. Soc.*, 2015, **137**, 13319–13324.
36 J. D. Grice and R. B. Ferguson, *Can. Mineral.*, 1974, **12**, 248–252.
37 J. Parise, *Acta Crystallogr. B: Struct. Sci. Cryst. Eng. Mater.*, 1980, **36**, 1179–1180.
38 S. Koenig, A. Eichhöfer, N. R. M. Crawford, R. Ahlrichs and D. Fenske, *Z. Anorg. Allg. Chem.*, 2007, **633**, 713–716.
39 The ^{1}H NMR spectrum of **1** is also consistent with the presence of four different PEt_3 environments, in a 4 : 2 : 3 : 2 ratio.
40 M. D. Walter, C. H. Booth, W. W. Lukens and R. A. Andersen, *Organometallics*, 2009, **28**, 698–707.
41 E. M. Schubert, *J. Chem. Educ.*, 1992, **69**, 62.
42 D. F. Evans, *J. Chem. Soc.*, 1959, 2003–2005.
43 Also present in this spectrum is a peak at 1200.0 *m*/*z*. The molecular weight and isotope pattern suggests it is an Ni_6 cluster, however a definitive formula could not be assigned.